Nonadiabatic Effects in the Two-Dimensional Infrared Spectra of Peptides: Application to Alanine Dipeptide

Thomas la Cour Jansen* and Jasper Knoester

Institute for Theoretical Physics and Materials Science Centre, University of Groningen, Nijenborgh 4, 9747 AG Groningen, The Netherlands

Received: July 27, 2006; In Final Form: September 5, 2006

A method of simulating two-dimensional infrared spectra accounting for nonadiabatic effects is presented. The method is applied to the amide I modes of a dipeptide. The information necessary to construct the time-dependent Hamiltonian for the system is extracted from molecular dynamics simulations using a recently published ab initio-based model. It is shown that the linear absorption spectrum agrees with experiment only if the nonadiabatic effects are accounted for. The two-dimensional infrared spectrum is predicted for a range of mixing times. It is shown that population transfer between the amide I site vibrations affects the anisotropy at longer mixing times. It is also demonstrated that the population transfer can, to a good approximation, be extracted from the simulated spectra using a procedure that should also be applicable to experimental spectra.

1. Introduction

Two-dimensional infrared correlation spectroscopy (2DIR)[1,2,3] is the infrared analogue of two-dimensional nuclear magnetic resonance (2DNMR).[4] The NMR technique has a tremendous resolution that enables the application of the method to resolve structures at the atomic level of small- and medium-sized proteins in solution, where hundreds of resonances and cross resonances are found in the spectra.[5] Although 2DIR does not have this high resolution, it has other advantages complimentary to 2DNMR. Operating with infrared light allows for the use of ultrashort pulses, providing time resolution in the femtosecond regime, which is orders of magnitude faster than 2DNMR. This makes it possible to follow the fastest chemical reactions, structural reorganizations, and vibrational energy redistribution in real time. Whereas typical NMR line shapes are narrow Lorentzians, because solvent fluctuations occur much faster than the spin precession, the 2DIR line shapes contain information about the solvent environment. In 2DIR, line shapes are observed all the way from the fast fluctuation limit, where the shapes are narrow Lorentzians, to the slow limit, where the shapes are elongated along the diagonal axis in the spectrum.[3]

In the typical 2DIR experiment, three infrared pulses are sent through the sample with short time delays between the pulses.[1−3] The first pulse brings the system into a coherent superposition of the ground state and a singly excited state. During the first time delay, t_1, the vibrations evolve in this coherent superposition. Fourier transforming with respect to t_1 gives the first frequency axis ω_1. The second pulse either brings the system back into the ground state, creates a singly excited state population, or creates a coherent superposition of two singly excited states. During the second time delay, t_2, the vibrations are evolving in either of these states. This time delay is called the mixing time. After the mixing time, the system is brought into another coherent superposition. This is either a coherent superposition between the ground state and a singly excited state or between a singly and a doubly excited state. This coherent superposition emits the detected signal that is frequency-resolved. The detected frequency gives the second frequency axis ω_3. The emission is not instantaneous, and the frequency ω_3 can be obtained by Fourier transforming the total emitted field as a function of the time t_3 elapsed after the mixing time.

Experimentally, 2DIR was first applied to investigate the structural signatures of proteins.[1] Later, generic signatures of the most common structural features have been established.[6−10] The technique was used to determine the angle between carbon monooxide ligands in a rhodium complex, demonstrating that one can obtain detailed structural information.[2] Since that time, spectra have been obtained for numerous compounds.[11−17] The studies of static structures rely only on the spectra obtained with the mixing time fixed at zero. Although these spectra do contain some information about the dynamics of the system, one only reaches the full potential of the technique by varying the mixing time. This was employed, for instance, to obtain the hydrogen bond lifetime of *N*-methyl acetamide (NMA) in different solvents[18] and the time scale of the transfer of vibrational OH stretch quanta between molecules in bulk water.[19]

Theoretically, most focus so far has been on spectra with the mixing time fixed at zero. A number of theoretical methods have been developed to simulate spectra. These differ in the amount of spectral dynamics that they are able to account for. The sum over states (SOS)[20,21] is the simplest method, but it does not account for dynamics. The nonlinear exciton equations (NEE)[20] can be used to calculate the spectra more efficiently, but this method, again, does not account for the dynamics. Both of these methods thus only account for the effect of static disorder on the line shape. The cumulant expansion for Gaussian fluctuations (CGF)[22,20,23] allows for describing the line shapes as long as the static frequency distribution is Gaussian and no vibrational transfer between different modes is present. The stochastic Liouville equation (SLE)[24] can be used to predict the dynamics if the fluctuations affecting the system are Markovian. The direct averaging of classical phase fluctuations (DCF)[24−26] can account for the dynamics as long as no vibrational transfer between different modes is present. Finally, all types of dynamics can, at least in principle, be accounted for by numerical integration of the Schrödinger equation (NISE).[24,27]

* To whom correspondence should be addressed. E-mail: t.l.c.jansen@rug.nl.

10.1021/jp064795t CCC: $33.50
Published on Web 10/14/2006

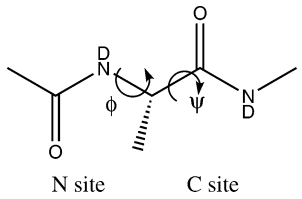

Figure 1. Structure of alanine dipeptide (ALDP). The Ramachandran angles ϕ and ψ are shown with arrows.

Although the latter method can account for more aspects of the dynamics, it is, as one could expect, also computationally more demanding.

In the present paper, we will use the NISE to simulate spectral dynamics accounting for everything from reorientational effects to frequency fluctuations and the vibrational transfer between modes. The method will be applied to simulate spectra of alanine dipeptide (ALDP, see Figure 1) in the amide I region. Because the NISE is computationally demanding, we will compare it to two approximate methods in order to find out how reliable they are and under which circumstances they can be applied.

We have chosen ALDP because it is an example of a small molecular system with interesting dynamic aspects. ALDP is a flexible peptide and the transition dipoles can thus change direction during the time delays between the applied laser pulses. This flexibility also results in fluctuations of the coupling between the two amide I oscillators in the peptide. Flexible alanine-based peptides have been the subject of previous molecular dynamics as well as 2DIR studies.[28−31] 2DIR and infrared absorption spectra for ALDP have been measured for different isotopomers of this peptide,[32] for $t_2 = 0$ and $t_2 = 500$ fs.

The 2DIR spectrum is determined by the fluctuating frequencies, anharmonicities, and transition dipoles of the two oscillators in ALDP, as well as the fluctuating coupling between them. The transition dipoles between the singly and doubly excited state of the same mode will be restricted to following the harmonic approximation, i.e., it will be in the same direction, but with a magnitude ratio of $\sqrt{2}$. The values for the fluctuating quantities are subsequently obtained from molecular dynamics simulations using an electrostatic map for the effect of the solvent water[26] combined with a map for the intrapeptide interactions.[33]

The remainder of this paper is organized as follows. In Section 2, the formalism is presented for calculating, using numerical integration of the Schrödinger equation, the population dynamics, the linear absorption, and 2DIR spectra, and polarization anisotropy. The results of the simulations are given and discussed in Section 3. Finally, conclusions are drawn in Section 4.

2. Theory

We employ the simplest possible exciton Hamiltonian for a collection of N floating oscillators of the form

$$\mathbf{H}(t) = \sum_{i=1}^{N}\left[\epsilon_i(t)\boldsymbol{b}_i^\dagger\boldsymbol{b}_i - \frac{\Delta_i(t)}{2}\boldsymbol{b}_i^\dagger\boldsymbol{b}_i^\dagger\boldsymbol{b}_i\boldsymbol{b}_i\right] + \sum_{i,j}^{N} J_{ij}(t)\boldsymbol{b}_i^\dagger\boldsymbol{b}_j + \sum_{i=1}^{N}\vec{\mu}_i(t)\vec{E}(t)[\boldsymbol{b}_i^\dagger + \boldsymbol{b}_i] \quad (1)$$

Here, $\epsilon_i(t)$ and $\Delta_i(t)$ are the fluctuating frequency and anharmonicity, respectively, of mode i, $J_{ij}(t)$ is the fluctuating coupling between two modes, and $\boldsymbol{b}_i^\dagger$ and $\boldsymbol{b}_i$ are the usual Bose creation and annihilation operators. The modes interact with the applied infrared electric field $\vec{E}(t)$ through the transition dipoles $\vec{\mu}_i(t)$, which might fluctuate in time as well. ALDP contains two amide I oscillators ($N = 2$). In the Hamiltonian (eq 1), states with a different number of excitations are only coupled when an external field is present. When the external field is vanishing, it is therefore block diagonal and the different blocks can be treated separately. We denote the block concerning the ground state $\mathbf{H}^{gg}$, the singly excited states $\mathbf{H}^{ee}$, and the doubly excited states $\mathbf{H}^{ff}$. We will consider interactions with an external electric field tuned to be resonant with the change of one excitation quantum. In this case, we need the transition dipoles between the ground state and the singly excited states μ^{ge} and those between the singly and doubly excited states μ^{ef}.

The time-dependent Schrödinger equation

$$\frac{\partial}{\partial t}\Phi(t) = -\frac{i}{\hbar}\mathbf{H}(t)\Phi(t) \quad (2)$$

is solved for each block independently. Here, $\Phi(t)$ is the wave function at time t. The evolution of all possible states can be tracked if the evolution is known in an arbitrary but fixed and complete basis. We will utilize the site basis, where the excitations are localized on the amide I sites. If a system was in the site basis state $\phi_i = \boldsymbol{b}_i^\dagger|g\rangle$ at time zero, it will have evolved into $\Phi_i(t)$ at time t. This wave function can be written in terms of the original fixed site basis functions ϕ for the considered excitation manifold.

$$\Phi_i(t) = \sum_j \phi_j \boldsymbol{c}_{ji}(t) \quad (3)$$

For $t = 0$, the expansion coefficients fulfill $c_{ji}(0) = \delta_{ji}$. Upon insertion of eq 3 in the time-dependent Schrödinger equation, an equation for the expansion coefficients is obtained

$$\frac{\partial}{\partial t}c_{ik}(t) = -\frac{i}{\hbar}\sum_j \mathbf{H}_{ij}(t)c_{jk}(t) \quad (4)$$

which can be written in matrix form

$$\frac{\partial}{\partial t}\boldsymbol{c}(t) = -\frac{i}{\hbar}\mathbf{H}(t)\boldsymbol{c}(t) \quad (5)$$

For numerical integration of this equation using small time increments, the Hamiltonian can be treated as a constant during each integration step. The integration over one such time step of duration Δt yields

$$\boldsymbol{c}((n+1)\Delta t) = \exp\left(-\frac{i}{\hbar}\mathbf{H}(n\Delta t)\Delta t\right)\boldsymbol{c}(n\Delta t) \equiv \mathbf{U}((n+1)\Delta t, n\Delta t)\boldsymbol{c}(n\Delta t) \quad (6)$$

with the integer n labeling the time step. By combining all time evolution operators $\mathbf{U}((j+1)\Delta t, n\Delta t)$ from the selected starting time to all other times, we have

$$\mathbf{U}(n\Delta t, 0) = [\prod_{m=1}^{m=n}\mathbf{U}(m\Delta t,(m-1)\Delta t)] \quad (7)$$

The product Π denotes the time-ordered operation from the left with increasing m. The time-evolution matrices between two arbitrary points in time are found using their unitary property $\mathbf{U}(t_1, t_0) = \mathbf{U}(t_1, 0)\mathbf{U}^\dagger(t_0, 0)$. Adding gg, ee, or ff to the matrices indicates which block of the Hamiltonian is used. The approach described here and the Hamiltonian employed allow for the description of population transfer within the exciton manifolds.

A. Population Transfer. The population transfer between two states in the site basis is calculated using

$$P_{ba}(t) = \langle |U_{ba}(t, 0)|^2 \rangle \tag{8}$$

where a is the initial state and b is the final state. Here and hereafter, $\langle \cdots \rangle$ denotes the ensemble average, which is obtained by summing over the contributions from configurations separated by 400 fs along the MD trajectory. At zero time delay, the population will be in the initial state, i.e., $P_{ab}(0) = \delta_{ab}$, and at infinite delay, the population will be equally distributed over all states, i.e., $P_{ab}(0) = 1/N$. The latter is due to the classical treatment of the bath, which is valid in the high-temperature limit, when the energy difference between the states is smaller than the thermal energy.

B. Linear Absorption. The linear absorption is given by the Fourier transform of the two-point correlation function of the transition dipole

$$I(\omega) = Im\int_0^\infty dt_1 \frac{i}{\hbar}\langle \mu^{ge}(\tau_2)\mathbf{U}^{ee}(\tau_2,\tau_1)\mu^{eg}(\tau_1)\rangle \exp(-i\omega t_1)\Gamma_{LA}(t_1) \tag{9}$$

Here, τ_2 and τ_1 are the times when the system interacts with the external field, and t_1 is the time between these interactions ($t_1 = \tau_2 - \tau_1$). The vibrational lifetime is accounted for by the relaxation factor

$$\Gamma_{LA}(t_1) = \exp(-t_1/2T_1) \tag{10}$$

where T_1 is the lifetime of the singly excited states.

C. 2DIR. 2DIR spectroscopy is a four wave mixing technique.[1−3] The 2DIR spectrum is given as the sum of the signal emitted in the directions with wave vectors $\bar{k}_I = -\bar{k}_1 + \bar{k}_2 + \bar{k}_3$ and $\bar{k}_{II} = \bar{k}_1 - \bar{k}_2 + \bar{k}_3$, where $\bar{k}_1$, $\bar{k}_2$, and $\bar{k}_3$ are the wave vectors of the incoming infrared fields. $\bar{k}_I$ is the photon-echo signal and $\bar{k}_{II}$ is the nonrephasing signal. Each of these signals contains three contributions from distinct Liouville space pathways: ground-state bleach (GB), stimulated emission (SE), and excited-state absorption (EA).[25,34] These are given by

$$S^{(I)}_{GB}(t_3, t_2, t_1) = -\left(\frac{i}{\hbar}\right)^3 \langle \mu^{ge}(\tau_1)\mathbf{U}^{ee}(\tau_1,\tau_2)\mu^{eg}(\tau_2)\mu^{ge}(\tau_4) \mathbf{U}^{ee}(\tau_4,\tau_3)\mu^{eg}(\tau_3)\rangle \Gamma_{GB}(t_3, t_2, t_1)$$

$$S^{(I)}_{SE}(t_3, t_2, t_1) = -\left(\frac{i}{\hbar}\right)^3 \langle \mu^{ge}(\tau_1)\mathbf{U}^{ee}(\tau_1,\tau_3)\mu^{eg}(\tau_3)\mu^{ge}(\tau_4) \mathbf{U}^{ee}(\tau_4,\tau_2)\mu^{eg}(\tau_2)\rangle \Gamma_{SE}(t_3, t_2, t_1)$$

$$S^{(I)}_{EA}(t_3, t_2, t_1) = \left(\frac{i}{\hbar}\right)^3 \langle \mu^{ge}(\tau_1)\mathbf{U}^{ee}(\tau_1,\tau_4)\mu^{ef}(\tau_4)\mathbf{U}^{ff}(\tau_4,\tau_3) \mu^{fe}(\tau_3)\mathbf{U}^{ee}(\tau_3,\tau_2)\mu^{eg}(\tau_2)\rangle \Gamma_{EA}(t_3, t_2, t_1)$$

$$S^{(II)}_{GB}(t_3, t_2, t_1) = -\left(\frac{i}{\hbar}\right)^3 \langle \mu^{ge}(\tau_4)\mathbf{U}^{ee}(\tau_4,\tau_3)\mu^{eg}(\tau_3)\mu^{ge}(\tau_2) \mathbf{U}^{ee}(\tau_2,\tau_1)\mu^{eg}(\tau_1)\rangle \Gamma_{GB}(t_3, t_2, t_1)$$

$$S^{(II)}_{SE}(t_3, t_2, t_1) = -\left(\frac{i}{\hbar}\right)^3 \langle \mu^{ge}(\tau_2)\mathbf{U}^{ee}(\tau_2,\tau_3)\mu^{eg}(\tau_3)\mu^{ge}(\tau_4) \mathbf{U}^{ee}(\tau_4,\tau_1)\mu^{eg}(\tau_1)\rangle \Gamma_{SE}(t_3, t_2, t_1)$$

$$S^{(II)}_{EA}(t_3, t_2, t_1) = \left(\frac{i}{\hbar}\right)^3 \langle \mu^{ge}(\tau_2)\mathbf{U}^{ee}(\tau_2,\tau_4)\mu^{ef}(\tau_4)\mathbf{U}^{ff}(t_3)\mu^{fe}(\tau_3) \mathbf{U}^{ee}(\tau_3,\tau_1)\mu^{eg}(\tau_1)\rangle \Gamma_{EA}(t_3, t_2, t_1) \tag{11}$$

The vibrational lifetime is included in an ad hoc way through the relaxation factors

$$\Gamma_{GB}(t_3, t_2, t_1) = \exp(-(t_3 + 2t_2 + t_1)/2T_1)$$

$$\Gamma_{SE}(t_3, t_2, t_1) = \exp(-(t_3 + 2t_2 + t_1)/2T_1)$$

$$\Gamma_{EA}(t_3, t_2, t_1) = \exp(-(t_3 + 2t_2 + t_1)/2T_1 - t_3/2T_2) \tag{12}$$

$\tau_1-\tau_4$ are the times for interactions with the external electric field and t_1-t_3 are the time delays between these (i.e., $t_1 = \tau_2 - \tau_1$, $t_2 = \tau_3 - \tau_2$, and $t_3 = \tau_4 - \tau_3$). T_1 and T_2 are the lifetimes of the singly and doubly excited states, respectively.

The signals are converted to the frequency domain using 2D Fourier transforms with respect to the time differences t_1 and t_3

$$S^{(I)}(\omega_3, t_2,\omega_1) = \int_0^\infty\int_0^\infty (S^{(I)}_{GB}(t_3, t_2, t_1) + S^{(I)}_{SE}(t_3, t_2, t_1) + S^{(I)}_{EA}(t_3, t_2, t_1))\exp(i(\omega_3 t_3 - \omega_1 t_1))dt_3 dt_1$$

$$S^{(II)}(\omega_3, t_2,\omega_1) = \int_0^\infty\int_0^\infty (S^{(II)}_{GB}(t_3, t_2, t_1) + S^{(II)}_{SE}(t_3, t_2, t_1) + S^{(II)}_{EA}(t_3, t_2, t_1))\exp(i(\omega_3 t_3 + \omega_1 t_1))dt_3 dt_1 \tag{13}$$

where t_2 is the mixing time. Finally, the 2DIR correlation spectrum is the imaginary part of the sum of the photon-echo and nonrephasing signals

$$I_{2D}(\omega_3, t_2,\omega_1) = Im(S^{(I)}(\omega_3, t_2,\omega_1) + S^{(II)}(\omega_3, t_2,\omega_1)) \tag{14}$$

The parallel and perpendicular polarization spectra were obtained using the proper averaging over polarization components of the transition dipole vectors as described elsewhere.[26,35]

D. Polarization Anisotropy and Population Dynamics. The polarization anisotropy is a useful measure for studying rotational and population dynamics. The anisotropy is defined by the normalized difference of the parallel and perpendicular polarized signals[36]

$$r(t) = \frac{S_{||}(t) - S_{\perp}(t)}{S_{||}(t) + 2S_{\perp}(t)} \tag{15}$$

For an isolated vibration, the change of the anisotropy is determined by the reorientation of the transition dipole moment.[36,37]

In an isotropic solution

$$r(t) = \frac{1}{5}\langle 3\cos^2(\Theta(t) - 1)\rangle \tag{16}$$

where $\Theta(t)$ is the angle between the transition dipole vector at two times separated by t. In this case, the anisotropy is a measure of the average rotation and can take values between −1/5 and 2/5. The latter value corresponds to no rotation and can be expected when the mixing time is zero. In systems of several coupled oscillators, the anisotropy can take any value because of interference effects.[37] Furthermore, the time evolution can be influenced by population transfer, moving the excitation from a vibration with transition dipole in one direction to another vibration with a different transition dipole direction.[19,27,36−39]

When the frequencies of the oscillators are well-separated, the population transfer can be followed relatively easily. This is much more difficult when the frequencies are strongly overlapping. As we will show below, however, under certain assumptions, the population transfer within a dimer can still be extracted from the anisotropy measurements by using additional

information that can be obtained, for example, using isotope labeling. If two oscillators give rise to an equally strong signal in the examined spectral region, the anisotropy can be approximated as

$$r(t) = (r_{AA}(t)P_{AA}(t) + r_{BB}(t)P_{BB}(t) + r_{BA}(t)P_{BA}(t) + r_{AB}(t)P_{AB}(t))/2 \quad (17)$$

Here r_{AA} and r_{BB} are the rotational correlation functions for each site defined as in eq 16, whereas r_{AB} and r_{BA} are the cross correlation functions defined similarly, but now taking the angle $\Theta(t)$ between the transition dipole of one oscillator at time zero and the transition dipole of the other one at time t. P_{AA} and P_{BB} are the probabilities of finding the population on the same site after the time delay and P_{AB} and P_{BA} are the probabilities that the population has transferred to the other site. Assuming that the sites are similar, we can use the same rotational correlation function $R(t) = r_{AA}(t) = r_{BB}(t)$ and the same survival probabilities $P(t) = P_{AA}(t) = P_{BB}(t)$. The cross correlation functions can be approximated by

$$R_X(t) = R_X(0)R(t)/R(0) = \langle 3\cos^2(\Theta_X) - 1\rangle R(t)/2 \quad (18)$$

where Θ_X is the angle between the two oscillators. This ensures that the cross correlation function at the initial time has the correct value depending only on the relative orientation of the transition dipoles and that at long times, it decays on the same time scale as the rotational correlation function. This leads to the expression

$$r(t) = R(t)P(t) + 0.5(1 - P(t))\langle 3\cos^2(\Theta_X) - 1\rangle R(t) \quad (19)$$

$R(t)$ can, to a good approximation, be replaced by the anisotropy of the isotope labeled species, where the frequencies of the two sites are separated, resulting in strong suppression of the population transfer and separate signals for the two sites. The factor $\langle 3\cos^2(\Theta_X) - 1\rangle$ can be obtained from the anisotropy in the cross-peak regions of the isotope-labeled spectra. Alternatively, it can be obtained if the structure is known from some other source.

From eq 19, it follows that in dimers, the approximate population transfer probability can be obtained by combining anisotropy measurements of isotope-labeled and unlabeled systems

$$P(t) = \frac{r(t) - 0.5\langle 3\cos^2(\Theta_X) - 1\rangle R(t)}{R(t) - 0.5\langle 3\cos^2(\Theta_X) - 1\rangle R(t)} \quad (20)$$

E. Adiabatic and Diabatic Approximations. When the basis states are well-separated and the coupling between them is smaller than their energy difference, they can be treated as being independent. This allows us to use a faster adiabatic scheme for calculating the response functions.[24] In the system we will consider, crossings of the site frequencies occur. However, this might not prevent use of an approximate scheme. In Figure 2, a typical avoided crossing is illustrated. When the frequencies of two oscillators cross, the coupling between them prevents the eigenstates from crossing. The shortest distance between the eigenstates will be twice the coupling constant. In the adiabatic scheme, one assumes that if one eigenstate was excited before the crossing, the same eigenstate will be excited after the crossing. Alternatively, a local-oscillator (diabatic) scheme can be used by assuming that if the state predominantly localized on one oscillator was excited before the crossing, the excitation will be in the state where this local oscillator has the most strength throughout the crossing. In the case of the avoided crossing illustrated in Figure 2, the excitation will thus jump from one eigenstate to the other at the point of the crossing. We tested these two approximations by diagonalizing the Hamiltonian for every snapshot in the trajectory and transforming the transition dipole matrices accordingly. The spectra were then calculated using eqs 7 and 9−16 given in ref 26 for the linear absorption and 2DIR spectra, respectively.

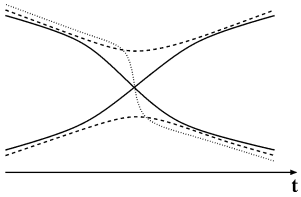

Figure 2. Avoided crossing arises when the site energies (full lines) cross. The coupling between the sites ensures that the eigenfrequencies (dashed lines) do not cross. In the slow limit, a system in an eigenstate will stay in that eigenstate and move along the dashed lines. In the fast limit, a system starting in one eigenstate will end up in the other, as illustrated by the dotted line. In general, the system will be in a superposition of the two states after passing the avoided crossing.

3. Results

Alanine dipeptide in heavy water was simulated using the GROMACS-3.14 program.[40] The SPC force field[41] was used for water and the OPLS force field[42] was used for the peptide. A simulation box with 1757 water molecules was constructed and equilibrated at 300 K. After equilibration, a 4 ns trajectory was obtained. The simulation was performed in the microcanonical ensemble with 2 fs time steps using constrained bond lengths and the LINCS algorithm.[43] Snapshots were saved for every 20 fs. The vibrational lifetimes T_1 and T_2 were set to 1800 fs.[44]

A trajectory of site frequencies, couplings, and transition dipoles was extracted from the MD trajectory using the method described in ref 33. This method includes the effect of the solvent fluctuations through the electric field and electric field gradient exerted by the solvent on the atoms participating in the amide I vibration. A DFT map relates the solvent shift with the electrostatic potential created by the solvent.[26] The frequency shifts due to the local structure characterized by the Ramachandran angles are accounted for using a DFT map that was constructed using glycine dipeptide.[33] The coupling between the two amide I oscillators of alanine dipeptide is obtained with a map, again relating this to the Ramachandran angles between the two peptide units.[33]

The simulation gives average frequencies of 1647.7 and 1653.3 cm^{-1} for the N and C sites, respectively. Using isotope labeling, we measured these frequencies to be 1631.5 and 1643 cm^{-1}.[32] The simulated spectrum will therefore be slightly blue shifted compared to the experimental spectrum, but with the peaks in the correct order. The average coupling was calculated to be 2.7 cm^{-1}, whereas measurements were found to be 1.5 ± 0.5 cm^{-1}.[32] The correlation between the N and C site frequencies is −0.056. This agrees with a picture of the frequency fluctuations being primarily due to the fluctuations of the directly hydrogen bound solvent water molecules, resulting in little correlation between frequencies at different sites. In Table 1, the parameters for a biexponential fit of the correlation function of the site frequencies and the coupling are given. For the site frequencies, the time constants are similar to those found for NMA in water.[18,26] The fluctuations are faster on the C site than on the N site. The magnitude of the coupling fluctuations is much smaller than that of the site frequencies and the

TABLE 1: Parameters for Biexponential Fits of the Frequency and Coupling Correlation Functions, $C(t) = \sigma^2(A_0\exp(-t/D_1) + (1 - A_0)\exp(-t/D_2))$

correlation	A_0	D_1 (fs)	D_2 (fs)	σ (cm^{-1})
N site	0.294	1525	82	18.96
C site	0.314	1005	69	18.65
coupling	0.575	3043	122	3.08

fluctuation times are slower. The average coupling and splitting between the sites are smaller than the fluctuation of the site frequencies; this holds for the experimental energy difference and coupling as well. This results in numerous crossings of the site frequencies as seen in Figure 3, where nonadiabatic effects can be expected to play an important role.

Figure 4 shows the calculated linear absorption along with the static distribution of eigenfrequencies and site frequencies and the experimentally observed spectrum.[32] In the spectrum obtained by the NISE, only one peak is observed. This is in agreement with experimental observation. The adiabatic model gives two clearly separated peaks, whereas the localized model gives a peak resembling the NISE calculation quite well. The static distribution of the adiabatic eigenstates shows one state at 1640 cm^{-1} and another at 1660 cm^{-1}. The two distinct peaks

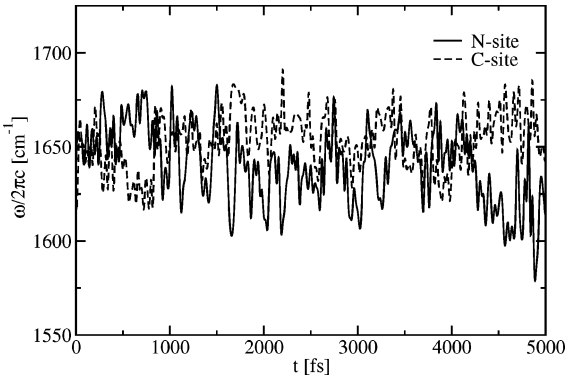

Figure 3. Fluctuating site frequencies using the modeling discussed in the text.

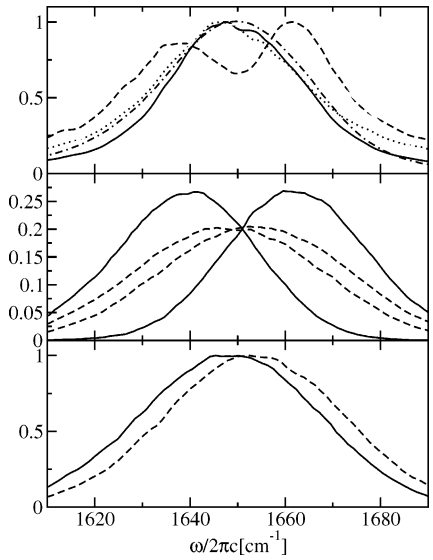

Figure 4. (Top) Calculated spectra using three approaches: NISE (solid line), adiabatic (dashed line), and localized states (dotted line), and the experimental spectrum[32] (dashed−dotted line) shifted by 13 cm^{-1} to the blue to ease comparison with the calculated spectra. (Middle) Static distribution of eigenvalues for the adiabatic approach (solid lines) and the localized states method (dashed lines). (Bottom) Static distribution of site frequencies. The solid line is the N site and the dashed one is the C site.

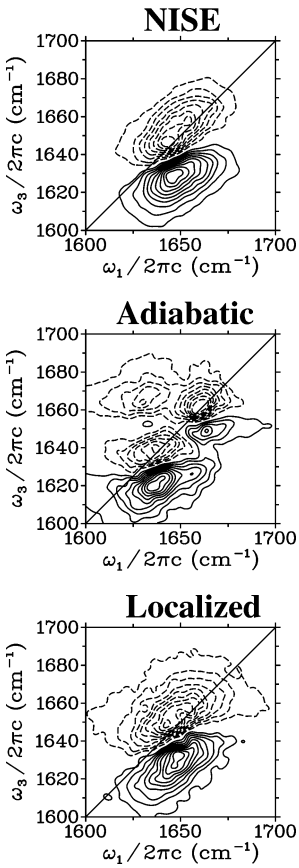

Figure 5. Perpendicular polarization 2DIR spectrum of alanine dipeptide simulated with mixing time zero obtained using three different methods. Dashed contour lines are negative (bleaching), full contour lines are positive (induced absorption). The contour lines reflect equidistant intensity levels.

arise because the two levels can never cross in the adiabatic approximation. The localized eigenstates, on the other hand, can cross and their distribution closely resembles the distribution of the site frequencies. Thus, the coupling in this system is so weak that the linear absorption can be well-approximated using the diabatic states. The spectrum obtained by the NISE agrees quite well with the experimental one. It is blue shifted by 13 cm^{-1} compared to the experiment, whereas its width is about 10% less (33.0 versus 37.6 cm^{-1}). The narrower width of the calculated spectrum can be explained by the smaller distance between the site frequencies obtained from the MD simulations.

The perpendicularly polarized 2DIR spectrum was simulated using the NISE, adiabatic, and localized models. The spectra for mixing time zero are shown in Figure 5. The NISE and localized models resemble each other, whereas more peaks are found in the spectrum calculated with the adiabatic approximation. This is analogous to what was observed for the linear absorption and shows the importance of nonadiabatic effects arising at the avoided crossings.

The 2DIR spectra were also calculated using the NISE for eight different values for the mixing time. The parallel and perpendicular polarized spectra for four of these times are shown in Figure 6. Visual inspection reveals little obvious difference between the spectra of the two polarization directions. Two not clearly separated peaks are observed in the ground state bleach-stimulated emission peak along the diagonal. These peaks are not resolved in the excited state absorption peak below the diagonal. At short mixing times, the peaks are stretched along the diagonal axis. At the longest time, the peaks have turned and are slightly elongated along the ω_1-axis, indicating that memory has disappeared. The time scale of the memory loss is

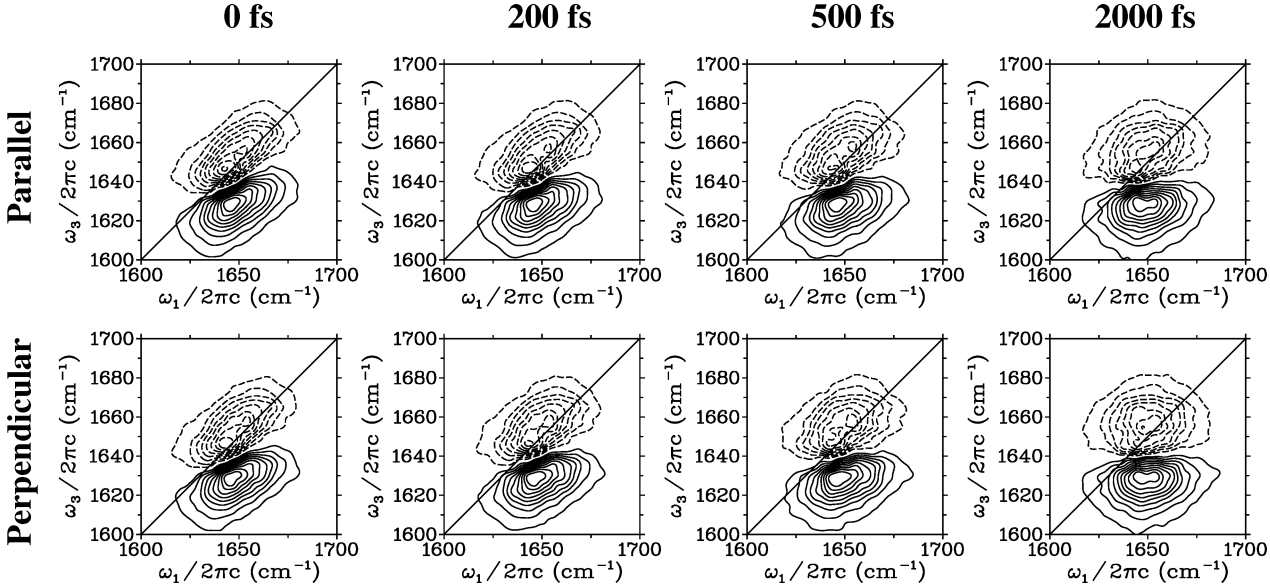

Figure 6. Simulated parallel and perpendicular polarization 2DIR spectra of alanine dipeptide with different mixing times. Dashed contour lines are negative (bleaching), full contour lines are positive (induced absorption). The contour lines reflect equidistant intensity levels.

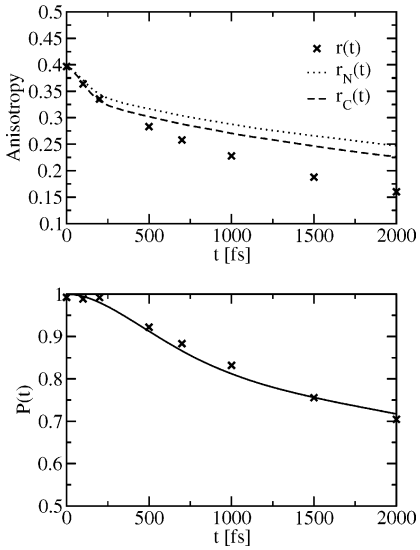

Figure 7. (Top) Crosses give the calculated anisotropy with broad pump and narrow probe (at 1660 cm^{-1}), the dotted (dashed) line is the rotational correlation function for the N site (C site) transition dipole. (Bottom) Population relaxation according to the full simulation, eq 8 (solid line), and as extracted from the simulated anisotropy, eq 20 (crosses).

consistent with the times reported for the frequency correlation functions (Table 1).

As discussed in Section 2, the anisotropy decay is a measure for the depolarization due to rotation of the dipoles and population transfer. The anisotropy corresponding to that obtained from a broad pump−narrow probe experiment was calculated by integrating the 2DIR spectra over ω_1 and selecting the signal for $\omega_3 = 1660$ cm^{-1}. The anisotropy was then obtained for different waiting times using eq 15. The calculated anisotropy is shown in Figure 7 along with the rotational correlation functions for the two transition dipoles of the sites. The anisotropy is seen to follow the rotational correlation functions during the first 250 fs. In this time interval, no population transfer takes place. At 500 fs, the anisotropy decays faster than the rotational correlation functions. This can only be explained by population transfer, which sets in on this time scale. On average, the angle between the two sites is 104 °, and population transfer will have a significant effect on the anisotropy. The population transfer is illustrated in Figure 7 by the probability of finding the excitation on one site, assuming that site was initially excited. This probability $P(t)$ was calculated using both the direct simulation of eq 8 and the approximate expression for extracting it from the anisotropy given in eq 20. In the latter method, $\langle 3\cos^2\Theta_X - 1\rangle$ was extracted directly from the simulation. The extracted probability follows the calculated one quite closely. This indicates both that the deviation of the anisotropy from the individual site rotational correlation function is (as observed in the top of Figure 7) due to population transfer and that the approximate way of extracting the population transfer from the anisotropy works.

A closer look at $P(t)$ reveals that, on average, half the excess population on an initially excited site is transferred to the other site in 1.6 ps. During the trajectory, an average of 11 avoided crossings occur each picosecond. This supports the observation in the spectral calculations that during avoided crossings, the population predominantly stays at the sites. Population is observed to flow back and forth between the sites at all times, resulting in the overall average population-transfer rate. No particularly strong avoided crossings responsible for the majority of the transfer were observed.

As is seen from Figure 7 (top panel) the rotational correlation function for the N site is decaying slower than that of the C site. This might seem counterintuitive, because the N site is located at the end of the dipeptide, whereas the C site is stuck in the middle, which one could think is more rigid and thus rotating slower. However, the lower frequency of the N site indicates that this site has stronger hydrogen bonding with the solvent, which can be caused by the larger solvent exposure. The slower decay of the N site rotational correlation function can thus be explained by the stronger bonding with the solvent water.

4. Conclusions

In this paper, using numerical integration of the Schrödinger equation, we presented the first simulation of linear absorption and 2DIR spectra of a peptide that includes nonadiabatic effects. We compared the resulting spectra with those obtained assuming that the dynamics follows either the adiabatic states or the localized (diabatic) dynamics. A comparison to experiment was made as well. Furthermore, 2DIR spectra were calculated for different mixing times. The dynamics was analyzed in terms of rotational motion and population dynamics.

The modeled site frequencies in ALDP were both blue shifted compared to the experimental values, with the N terminal site having a slightly larger shift than the C terminal site. The average simulated coupling was about one wave number larger than the one obtained from the experiment. It has been shown that existing MD force fields sample peptide configurations as well as the abundance of hydrogen bonding between the peptide and solvent with only a limited accuracy.[26,29] More accurate force fields, including, for example, polarization effects, are likely to improve the already good agreement with experimental findings. Part of the blue shift of the simulated frequencies can be explained by the neglect of dispersion forces in the maps connecting the frequencies. In systems with large dispersion forces, this should be accounted for, but the effect is minor here.

The site frequencies were found to be practically uncorrelated, which finds its origin in the fact that the largest fluctuation in the frequencies arises from the hydrogen-bonded solvent water.

In accordance with experimental observation[32] the calculated linear absorption spectrum shows only one peak. The adiabatic approximation was shown to fail in predicting the one-peak structure. This is attributed to the large magnitude of the frequency fluctuations compared to the small site frequency separation and coupling. The failure of the adiabatic approximation means that the DCF and CGF methods employing this approximation can be expected to fail for this and similar systems, at least if the eigenstates are used as a basis. In the calculated 2D spectra, the failure of the adiabatic approximation was just as evident.

The 2DIR spectra were calculated for different mixing times. At short times, a two-peak structure on the diagonal is visible; however, the peaks are barely resolved. In the excited state absorption, no subpeaks are resolved. Within 2 ps, the initial diagonally elongated peak shape, reflecting an inhomogeneous distribution of frequencies, has changed into a peak shape with a horizontal node corresponding to a homogeneous distribution of frequencies. This time scale agrees well with the decay of the simulated frequency correlation functions.

The polarization anisotropy calculated for a pump−probe experiment exhibits a fast initial decay due to orientational change of the site transition dipoles and a decay at a longer time scale largely determined by the population transfer from one site to the other. This is the first time the effect of population transfer between two peptide sites on the anisotropy has been simulated. It was further shown that the population transfer can, at least approximately, be extracted from the anisotropy even in this case, where the signals of the two oscillators are not spectrally resolved.

We showed that nonadiabatic effects have a clear effect on both the linear absorption and the 2DIR spectra of alanine dipeptide. The presented method, although computationally more demanding than methods ignoring these effects, can still be applied to more complex systems than the dimer. It is not yet clear what the impact is on peptides and proteins, but one would assume that the effects grow, because the spectra get congested and population transfer to multiple states can take place. This matter is currently under investigation for a 12-residue β-hairpin.

Acknowledgment. T.l.C.J. acknowledges The Netherlands Organization for Scientific Research (NWO) for support through a VENI grant. The authors thank Andrei Tokmakoff and Ziad Ganim for helpful discussions. Robin M. Hochstrasser and Yung Sam Kim are gratefully acknowledged for providing the experimental data.

References and Notes

(1) Hamm, P.; Lim, M. H.; Hochstrasser, R. M. *J. Phys. Chem. B* **1998**, *102*, 6123.
(2) Golonzka, O.; Khalil, M.; Demirdöven, N.; Tokmakoff, A. *Phys. Rev. Lett.* **2001**, *86* (10), 2154−2157.
(3) Mukamel, S. *Annu. Rev. Phys. Chem.* **2000**, *51*, 691.
(4) Hahn, E. L. *Phys. Rev.* **1950**, *80*, 580.
(5) Stryer, L.; Tymoczko, J. L.; Berg, J. M. *Biochemistry*, 5th ed.; Freeman: New York, 2002.
(6) Demirdöven, N.; Cheatum, C. M.; Chung, H. S.; Khalil, M.; Knoester, J.; Tokmakoff, A. *J. Am. Chem. Soc.* **2004**, *126* (25), 7981−7990.
(7) Abramavicius, D.; Zhuang, W.; Mukamel, S. *J. Phys. Chem. B* **2004**, *108* (108), 18034.
(8) Woutersen, S.; Hamm, P. *J. Chem. Phys.* **2001**, *115*, 7737.
(9) Ham, S.; Hahn, S.; Lee, C.; Kim, T.-K.; Kwac, K.; Cho, M. *J. Phys. Chem. B* **2004**, *108*, 9333.
(10) Maekawa, H.; Toniolo, C.; Moretto, A.; Broxterman, Q. B.; Ge, N.-H. *J. Phys. Chem. B* **2006**, *110*, 5835.
(11) Asbury, J. B.; Steinel, T.; Kwac, K.; Corcelli, S. A.; Lawrence, C. P.; Skinner, J. L.; Fayer, M. D. *J. Chem. Phys.* **2004**, *121*, 12431.
(12) Asbury, J. B.; Steinel, T.; Stromberg, C.; Gaffney, K. J.; Piletic, I. R.; Goun, A.; Fayer, M. D. *Chem. Phys. Lett.* **2003**, *374* (3−4), 362−371.
(13) Zanni, M. T.; Asplund, M. C.; Hochstrasser, R. M. *J. Chem. Phys.* **2001**, *114* (10), 4579−4590.
(14) Krummel, A. T.; Mukherjee, P.; Zanni, M. T. *J. Phys. Chem. B* **2003**, *107* (35), 9165−9169.
(15) Eaves, J. D.; Loparo, J. J.; Fecko, C. J.; Roberts, G. M.; Tokmakoff, A.; Geiger, L. C. *Proc. Natl. Acad. Sci. U.S.A.* **2005**, *102*, 13019.
(16) Larsen, O. F. A.; Bodis, P.; Buma, W. J.; Hannam, J. S.; Leigh, D. A.; Woutersen, S. *Proc. Natl. Acad. Sci. U.S.A.* **2005**, *102*, 13379.
(17) Volkov, V.; Chelli, R.; Righini, R. *J. Phys. Chem. B* **2006**, *110*, 1499.
(18) DeCamp, M. F.; DeFlores, L.; McCracken, J. M.; Tokmakoff, A.; Kwac, K.; Cho, M. *J. Phys. Chem. B* **2005**, *109*, 11016.
(19) Cowan, M. L.; Bruner, B. D.; Huse, N.; Dwyer, J. R.; Chugh, B.; Nibbering, E. T. J.; Elsaesser, T.; Miller, R. J. D. *Nature (London)* **2005**, *434*, 199.
(20) Mukamel, S.; Abramavicius, D. *Chem. Rev.* **2004**, *104*, 2073.
(21) Cheatum, C. M.; Tokmakoff, A.; Knoester, J. *J. Chem. Phys.* **2004**, *120*, 8201.
(22) Mukamel, S. *Phys. Rev. A* **1983**, *28*, 3480.
(23) Hahn, S.; Ham, S.; Cho, M. *J. Phys. Chem. B* **2005**, *109*, 11789.
(24) Jansen, T. l. C.; Zhuang, W.; Mukamel, S. *J. Chem. Phys.* **2004**, *121*, 10577.
(25) Kwac, K.; Lee, H.; Cho, M. *J. Chem. Phys.* **2004**, *120*, 1477.
(26) Jansen, T. l. C.; Knoester, J. *J. Chem. Phys.* **2006**, *124*, 044502.
(27) Torii, H. *J. Phys. Chem. A* **2006**, *110*, 4822.
(28) Woutersen, S.; Pfister, R.; Hamm, P.; Mu, Y.; Kosov, D. S.; Stock, G. *J. Chem. Phys.* **2002**, *117*, 6833.
(29) Mu, Y.; Kosov, D. S.; Stock, G. *J. Phys. Chem. B* **2003**, *107*, 5064.
(30) Gorbunov, R. D.; Kosov, D. S.; Stock, G. *J. Chem. Phys.* **2005**, *122*, 224904.
(31) Gnanakaran, S.; Garcia, A. E. *J. Phys. Chem. B* **2003**, *107*, 12555.
(32) Kim, Y. S.; Wang, J.; Hochstrasser, R. M. *J. Phys. Chem. B* **2005**, *109*, 7511.
(33) Jansen, T. l. C.; Dijkstra, A. G.; Watson, T. M.; Hirst, J. D.; Knoester, J. *J. Chem. Phys.* **2006**, *125*, 044312.
(34) Mukamel, S. *Principles of Nonlinear Optical Spectroscopy*; Oxford University Press: New York, 1995.
(35) Hochstrasser, R. M. *Chem. Phys.* **2001**, *266* (2−3), 273−284.
(36) Fleming, G. R. *Chemical Applications of Ultrafast Spectroscopy*; Oxford University Press: Oxford, U.K., 1985.
(37) Jonas, D. M.; Lang, M. J.; Nagasawa, Y.; Joo, T.; Fleming, G. R. *J. Phys. Chem.* **1996**, *100*, 12660.
(38) Woutersen, S.; Bakker, H. J. *Nature (London)* **1999**, *402*, 507.
(39) Torii, H. *J. Phys. Chem. A* **2006** *110*, 9469.
(40) Berendsen, H. J. C.; van der Spoel, D.; van Drunen, R. *Comput. Phys. Commun.* **1995**, *91*, 43.
(41) Berendsen, H. J. C.; Grigera, J. R.; Straatsma, T. P. *J. Phys. Chem.* **1987**, *91*, 6269.
(42) Jorgensen, W. L.; Tirado-Rives, J. *J. Am. Chem. Soc.* **1988**, *110*, 1657.
(43) Hess, B.; Bekker, H.; Berendsen, H. J. C.; Fraaije, J. G. E. M. *J. Comput. Chem.* **1997**, *18*, 1463.
(44) Woutersen, S.; Mu, Y.; Stock, G.; Hamm, P. *Chem. Phys.* **2001**, *266*, 137.